Pergamon

Int. J. Solids Structures Vol. 31, No. 8, pp. 1113–1131, 1994

0020-7683/94 $6.00 + .00

AN ANISOTROPIC FRICTION AND WEAR MODEL

Z. MRÓZ and S. STUPKIEWICZ
Institute of Fundamental Technological Research, Warsaw, Poland

(*Received* 25 *May* 1993; *in revised form* 21 *October* 1993)

Abstract—The classical Coulomb friction condition and the sliding rule are generalized in order to account for friction anisotropy. A model of two surfaces with anisotropic layout of asperities interacting elastically is first considered in order to generate limit friction condition and a sliding rule. Next, a class of phenomenological models is considered in order to simulate anisotropic friction, sliding and wear rate of contacting surfaces.

1. INTRODUCTION

A classical Coulomb condition can be visualized by a rigid block model sliding within the contact plane when the limit friction state is reached. The sliding velocity is then predicted by the normality rule associated with the sliding potential. If there is no dilatancy assumed at the contact, the velocity potential differs from the limit friction condition, thus predicting only tangential velocity components. However, the normality (or associated sliding rule) is usually assumed to be valid within the tangential force plane for a specified normal contact force. Such sliding rules were discussed by Michałowski and Mróz (1978) and Curnier (1984). A more general mathematical structure of sliding rules for various classes of contact anisotropy was discussed by Zmitrowicz (1987, 1989), who, however, did not postulate any interrelation between the limit friction condition and the sliding potential.

By considering a model of rigid anisotropic asperities, it was shown in Michałowski and Mróz (1978) that, in general, a non-associated sliding rule within the contact plane occurs with possible concavity of the limit friction surface. Some experimental data concerned with the directional sliding effects in anisotropic friction were provided by Halaunbrenner (1960) and Rabinowicz (1957). The hysteretic effects occurring at contact during cyclic loading were discussed by Jarzębowski and Mróz (1994) and a more general constitutive model accounting for hysteretic phenomena and both contact dilatancy and compaction was proposed by Mróz and Jarzębowski (1994).

The aim of this paper is to extend further the analysis of Michałowski and Mróz (1978) and to present a unified description of limit friction condition, sliding rule and wear rate for a class of non-isotropic contact states. Only velocity-independent friction effects are considered and both normal and tangential elastic contact compliances are neglected. The slip–stick phenomena, typical for velocity-dependent friction models [cf., for instance, Haessig and Friedland (1991)] are not considered in this paper. Also the hysteretic effects occurring during cyclic loading are not accounted for. The present formulation will therefore provide a description of advanced sliding when the contact interface reaches its steady-state for the specified normal pressure [or "critical state", in the terminology of Jarzębowski and Mróz (1994)].

In the next section, a simple asperity model is discussed in order to obtain an insight into the character of sliding rules and their relation to limit friction conditions. Section 3 is concerned with a class of anisotropic friction models and in Section 4 the wear models are proposed by assuming the dependence of wear rate on the specific dissipation rate. Some particular representations and applications are discussed in Section 5.

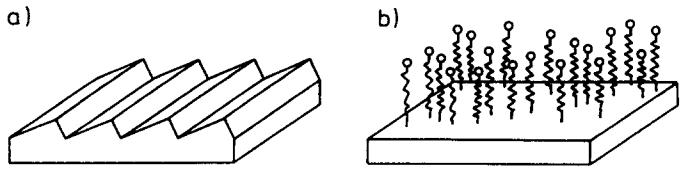

Fig. 1. Asperity model of orthotropic friction: (a) orthotropic surface with parallel wedge asperities; (b) plane with isotropically distributed spring asperities.

2. AN ASPERITY MODEL OF ORTHOTROPIC FRICTION

Consider a model of two contacting surfaces one of which has long wedge-shaped asperities specified by the angles φ_1, φ_2 (Fig. 1), the other having isotropically distributed asperities modelled by a set of parallel springs of uniform stiffness and distribution, attached to the upper moving plate. During the contact and relative sliding, the springs are assumed to contract or extend and slide along the wedge asperities so that the overall motion of the sliding body occurs parallel to the nominal contact plane. We neglect the flexural compliance of springs, and assume the longitudinal compliance of springs to be equal to $1/k$.

Consider first a single spring interaction with the wedge asperity. Referring to Fig. 2(a), consider an inclined plane Π representing the wedge asperity and the nominal plane Π_r. The rectangular coordinate system x, y, z specifies the plane Π_r and the system ξ, η specifies the plane Π. The sliding velocity vector v_0 within the Π-plane has the components $v_\xi = v_0 \cos\beta_0$, $v_\eta = v_0 \sin\beta_0$. The projected velocity vector $\mathbf{v}$ within the Π_r-plane has its components $v_x = v\cos\beta$, $v_y = v\sin\beta$, so we have in the x, y, z-system

$$\mathbf{v}_0 = [v\cos\beta,\ v\sin\beta,\ v\cos\beta\tan\varphi]^T, \quad \mathbf{v} = [v\cos\beta,\ v\sin\beta, 0]^T, \quad \tan\beta_0 = \tan\beta\cos\varphi. \tag{1}$$

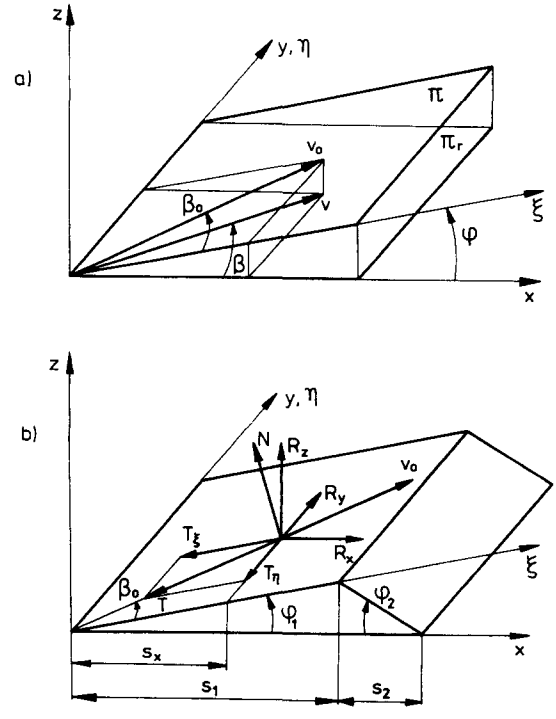

Fig. 2. Asperity model of orthotropic friction: (a) velocity vectors $\mathbf{v}$ and $\mathbf{v}_0$; (b) contact forces T and N acting on a single spring asperity and reactions R_x, R_y, R_z.

The spring–wedge interaction forces N and $T = \mu N$ are equilibrated by the forces R_x, R_y and R_z applied to the moving plate. We have

$$R_z = N\cos\varphi - T_\xi \sin\varphi, \quad R_x = N\sin\varphi + T_\xi\cos\varphi, \quad R_y = T_\eta, \tag{2}$$

where $T_\xi = T\cos\beta_0$ and $T_\eta = T\sin\beta_0$. The vertical force R_z is related to spring displacement $u = u_0 + s_x\tan\varphi$ by the relation $R_z = ku$. Here u_0 denotes the spring displacement at the bottom position of asperity and s_x denotes the contact position component along the x-axis (Fig. 2(b)). It is assumed that there is no separation of springs and wedge asperities and the lowest spring force at the asperity bottom is $R_z = ku_0 > 0$, where compressive forces are assumed as positive. From (2) we have

$$N = ku\left[\cos\varphi - \frac{\mu\tan\varphi\cos\beta}{\sqrt{1+\tan^2\varphi\cos^2\beta}}\right]^{-1} \tag{3}$$

and since $0 \leqslant N < \infty$, the following inequality

$$\cos\varphi - \frac{\mu\tan\varphi\cos\beta}{\sqrt{1+\tan^2\varphi\cos^2\beta}} > 0 \tag{4}$$

provides the admissible range of variations of μ and φ.

Inequality (4) can be used to limit the critical friction coefficient, thus

$$\mu < \mu_{cr} = \frac{\cos^2\varphi}{\sin\varphi}\sqrt{1/\cos^2\beta + \tan^2\varphi}. \tag{5}$$

This inequality is satisfied for all slip orientations β when

$$\mu < \mu_{cr} = \cot\varphi. \tag{6}$$

Equations (2) provide the components of tangential force expressed in terms of the normal force R_z

$$\begin{aligned} R_x &= ku\frac{\sin\varphi\sqrt{1+\tan^2\varphi\cos^2\beta} + \mu\cos\beta}{\cos\varphi\sqrt{1+\tan^2\varphi\cos^2\beta} - \mu\tan\varphi\cos\beta} = R_z H_x(\mu,\varphi,\beta) \\ R_y &= ku\frac{\mu\sin\beta}{\cos\varphi\sqrt{1+\tan^2\varphi\cos^2\beta} - \mu\tan\varphi\cos\beta} = R_z H_y(\mu,\varphi,\beta) \\ R_z &= ku. \end{aligned} \tag{7}$$

Consider now a uniformly distributed set of springs interacting with both sides of wedge asperities. The specific values of normal and tangential forces (per unit area of the reference plane) acting on the moving plate now are

$$\begin{aligned} N &= \frac{\lambda}{\lambda+1}R_N^{(1)} + \frac{1}{\lambda+1}R_N^{(2)} = R_N \\ T_x &= \frac{\lambda}{\lambda+1}T_x^{(1)} + \frac{1}{\lambda+1}T_x^{(2)} \\ T_y &= \frac{\lambda}{\lambda+1}T_y^{(1)} + \frac{1}{\lambda+1}T_y^{(2)}, \end{aligned} \tag{8}$$

where $R_N^{(1)} = R_N^{(2)} = R_N$ are the mean values of specific normal forces acting on respective

sides of wedge asperities. Similarly, $T_x^{(1)}$, $T_x^{(2)}$, $T_y^{(1)}$, $T_y^{(2)}$ are the mean values of specific tangential forces. Further, we have

$$\lambda = \frac{s_1}{s_2} = \frac{\tan\varphi_1}{\tan\varphi_2}, \qquad R_N = k(u_0 + \tfrac{1}{2}h)$$
$$T_x^{(1)} = R_N H_x(\mu, \varphi_1, \beta), \quad T_x^{(2)} = R_N H_x(\mu, -\varphi_2, \beta)$$
$$T_y^{(1)} = R_N H_y(\mu, \varphi_1, \beta), \quad T_y^{(2)} = R_N H_y(\mu, -\varphi_2, \beta) \tag{9}$$

and s_1, s_2 and $h = s_1 \tan\varphi_1 = s_2 \tan\varphi_2$ are shown in Fig. 2(b). Equations (8) provide us the orientation of the specific tangential force with respect to the velocity vector $\boldsymbol{v}$.

Consider a particular case when $\varphi_1 = \varphi_2 = \varphi$ so the friction limit surface is symmetric with respect to the origin. In a more general case $\varphi_1 \neq \varphi_2$ this symmetry is not preserved. Relations (8) now provide

$$T_x = \mu_x N, \quad T_y = \mu_y N, \quad N = k(u_0 + \tfrac{1}{2}h) \tag{10}$$

and

$$\mu_x = \mu \frac{\cos\beta}{\cos\varphi} \frac{\sqrt{1+\tan^2\varphi\cos^2\beta}}{1-\sin^2\varphi\sin^2\beta-\mu^2\tan^2\varphi\cos^2\beta} = \mu_x(\beta, \varphi, \mu)$$
$$\mu_y = \mu \sin\beta\cos\varphi \frac{\sqrt{1+\tan^2\varphi\cos^2\beta}}{1-\sin^2\varphi\sin^2\beta-\mu^2\tan^2\varphi\cos^2\beta} = \mu_x(\beta, \varphi, \mu). \tag{11}$$

Equations (11) imply the following relationship between orientations of $\boldsymbol{v}$ and $\mathbf{T}$

$$\tan\alpha = \frac{T_y}{T_x} = \cos^2\varphi\tan\beta, \quad \tan\beta = \frac{v_y}{v_x}. \tag{12}$$

The principal friction coefficients now are

$$\alpha = \beta = 0: \quad \mu_1 = \mu_x = \frac{\mu}{1-(1+\mu^2)\sin^2\varphi}$$
$$\alpha = \beta = \frac{\pi}{2}: \quad \mu_2 = \mu_y = \frac{\mu}{\cos\varphi} \tag{13}$$

so that

$$\frac{\mu_2}{\mu_1} = (1+\mu^2)\cos\varphi - \frac{\mu^2}{\cos\varphi} \leqslant 1. \tag{14}$$

Let us note that the velocity potential is now an ellipse with its principal axes coinciding with the orthotropy axes x, y

$$G(T_x, T_y) = \left[\left(\frac{T_x}{d_1}\right)^2 + \left(\frac{T_y}{d_2}\right)^2\right]^{1/2} - 1 = 0, \quad \frac{d_2}{d_1} = \cos\varphi. \tag{15}$$

In fact, the sliding rule generated by (15) is

$$v_x = \lambda \frac{\partial G}{\partial T_x} = \lambda \frac{T_x}{d_1^2}, \quad v_y = \lambda \frac{\partial G}{\partial T_y} = \lambda \frac{T_y}{d_2^2}, \quad \lambda > 0 \tag{16}$$

and

$$\tan \beta = \frac{v_y}{v_x} = \frac{T_y}{T_x}\left(\frac{d_1}{d_2}\right)^2 = \frac{\tan \alpha}{\cos^2 \varphi} \tag{17}$$

which verifies (12). On the other hand, the limit friction condition in the (T_x, T_y)-plane is not represented by an ellipse, so the sliding rule is not associated with the limit friction condition. In view of (12), the limit condition can be presented as follows:

$$T = Nf(\alpha), \tag{18}$$

where

$$f(\alpha) = \frac{\mu}{\cos \varphi} \frac{\sqrt{\cos^2 \varphi \cos^2 \alpha + \sin^2 \alpha}}{\sin^2 \alpha + [1 - (1+\mu^2) \sin^2 \varphi] \cos^2 \alpha}. \tag{19}$$

Figure 3 shows the diagram $f = f(\alpha)$ for varying values of μ and φ. It is seen that the limit friction curves are close to ellipses of ratios of principal axes different from the ratio specified by (15) for the sliding potential ellipse.

Let us now approximate the limit friction condition by an ellipse with its axes following orthotropy axes and use (15) as the sliding potential. Therefore, we have

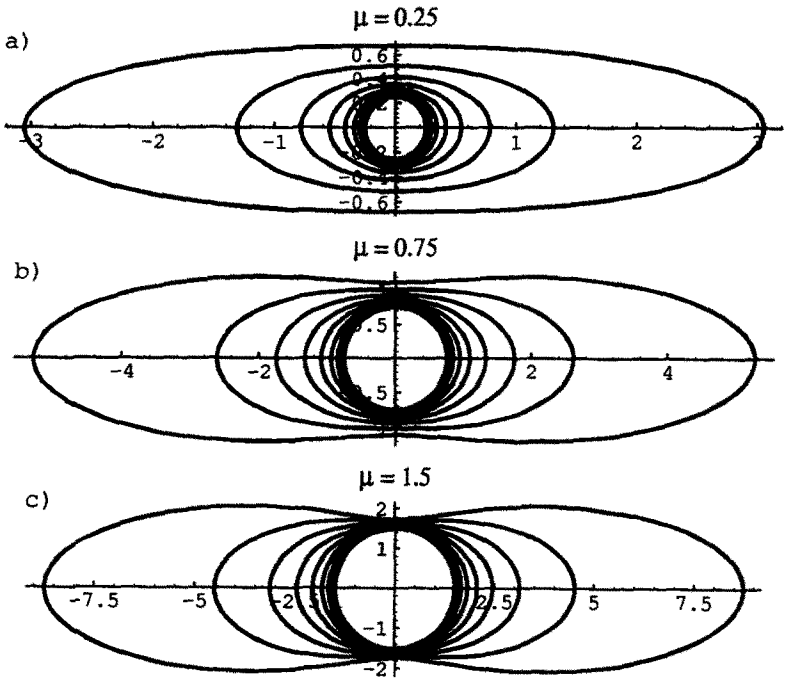

Fig. 3. Limit friction curves generated by the asperity model: (a) $\mu = 0.25$; (b) $\mu = 0.75$; (c) $\mu = 1.5$; for angle φ varying from $\varphi = 0$ (circles) to $\varphi = 0.9 \arctan \mu$.

$$F(T_x, T_y, N) = \left[\left(\frac{T_x}{c_1}\right)^2 + \left(\frac{T_y}{c_2}\right)^2\right]^{1/2} - N = 0$$

$$G(T_x, T_y, N) = \left[\left(\frac{T_x}{d_1}\right)^2 + \left(\frac{T_y}{d_2}\right)^2\right]^{1/2} - N = 0. \tag{20}$$

Assume that $c_1 = \mu_1$ and $c_2 = \mu_2$ so the principal ellipse axes are determined by the friction rules (18) and (19). Assume further that

$$\frac{d_2}{d_1} = \left(\frac{c_2}{c_1}\right)^p = \left(\frac{\mu_2}{\mu_1}\right)^p \tag{21}$$

so the principal axes ratio of sliding potential is related to the axes ratio of the limit friction ellipse. If the sliding rule (12) derived from the asperity interaction model is to be satisfied, we obtain

$$\tan\alpha = \left(\frac{d_2}{d_1}\right)^2 \tan\beta = \left(\frac{\mu_2}{\mu_1}\right)^{2p} \tan\beta = \cos^2\varphi \tan\beta \tag{22}$$

and in view of (14), there is

$$p = \frac{\ln(\cos\varphi)}{\ln[(1+\mu^2)\cos\varphi - \mu^2/\cos\varphi]}. \tag{23}$$

For $p = 1$ the case of associated sliding rule is obtained for which the limit friction curve and the sliding potential coincide within the (T_x, T_y)-plane. For $p < 1$, we obtain a class of sliding rules dependent on the asperity angle φ and the friction coefficient μ. Figure 4 presents the diagram of variation of the non-associativity parameter p as a function of φ and μ.

The present interaction model, although very simplified, provides a valuable insight into the character of limit friction and sliding rules. It is seen that the normality rule does not occur within the tangential force plane, and the sliding potential can be represented by

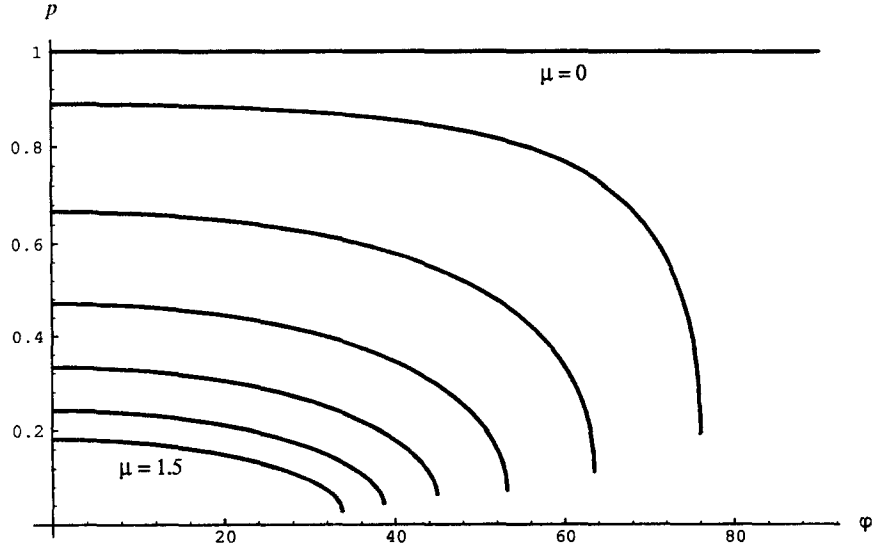

Fig. 4. Variation of the scaling parameter p resulting from the asperity model as a function of φ for different values of μ.

an ellipse of different axes ratio than that of principal friction coefficients. Further extensions of this model could provide more information. In particular, a non-linear contact compliance could be generated by considering consecutive engagement of springs and wedge asperities under normal compression. Further, the spring asperities could be assumed to possess both axial and flexural compliance with possible dynamic snaps when passing from one to the other asperity side. This micromechanical aspect of contact response will be discussed in a separate paper.

3. GENERAL ANISOTROPIC FRICTION MODEL

Assuming a velocity-independent friction model and a linear dependence of the limit tangential force on normal force, the generalized Coulomb friction condition has the form

$$F(T_x, T_y, N) = T - Nf(\alpha) = 0, \tag{24}$$

where α denotes the angle of the tangential force **T** with the x-axis of the Cartesian reference system, so that $T_x = T\cos\alpha$, $T_y = T\sin\alpha$ (Fig. 5). The sliding velocity vector v is inclined at the angle β to the x-axis, so that

$$\tan\alpha = \frac{T_y}{T_x}, \quad \tan\beta = \frac{v_y}{v_x}, \quad \beta = h(\alpha). \tag{25}$$

The sliding rule is therefore specified once the function $\beta = h(\alpha)$ is determined. It is natural to expect that along the anisotropy symmetry axes, there should be $\beta = \alpha$.

It is convenient to formulate the sliding rule by using the convex slip potential

$$G(T_x, T_y, N) = T - Ng(\alpha) = 0 \tag{26}$$

with the sliding rule

$$v_x = \lambda\frac{\partial G}{\partial T_x} = \lambda\left(\cos\alpha + \frac{g'}{g}\sin\alpha\right), \quad v_y = \lambda\frac{\partial G}{\partial T_y} = \lambda\left(\sin\alpha - \frac{g'}{g}\cos\alpha\right), \tag{27}$$

where g' denotes the derivative with respect to α, and the multiplier λ is obtained from the relation $v^2 = v_x^2 + v_y^2$, namely

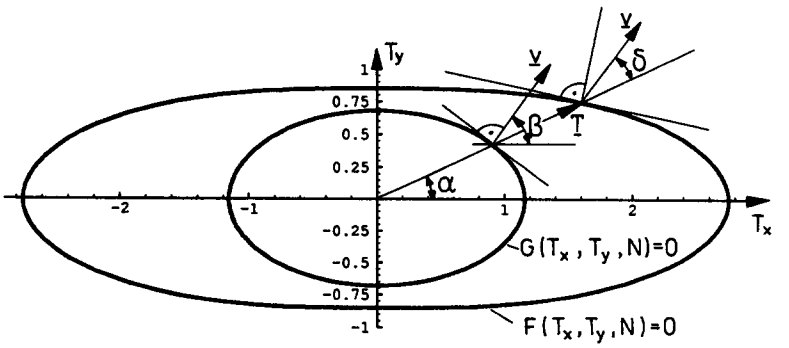

Fig. 5. Friction and sliding rules generated by the limit friction surface $F(T_x, T_y, N) = 0$ and the sliding potential $G(T_x, T_y, N) = 0$.

$$\lambda = v\left[1+\left(\frac{g'}{g}\right)^2\right]^{-1/2}. \tag{28}$$

We have $f(\alpha) = g(\alpha)$ for the associated slip rule and the formulae (27) and (28) are valid with $g(\alpha)$ replaced by $f(\alpha)$.

The relation between α and β can now be presented in the following form

$$\tan(\alpha-\beta) = \tan\delta = \frac{g'}{g} \quad \text{or} \quad \beta = \alpha-\delta = \alpha-\arctan\left(\frac{g'}{g}\right), \tag{29}$$

where δ denotes the angle between the friction force and velocity vectors $\mathbf{T}$ and $\mathbf{v}$ (Fig. 5).

The dissipation function is specified as follows:

$$D = T_x v_x + T_y v_y = \lambda N f(\alpha) = Nvf\left[1+\left(\frac{g'}{g}\right)^2\right]^{-1/2} = Nvd(\alpha) = Nv\bar{d}(\beta), \tag{30}$$

where $\bar{d}(\beta) = d[\alpha(\beta)]$.

Let us introduce the limit force components T_n and T_t parallel and normal to the sliding velocity v and the respective friction coefficients t_n and t_t. We have

$$T_n = \frac{D}{v} = Nf\left[1+\left(\frac{g'}{g}\right)^2\right]^{-1/2},$$

$$T_t = T_n \tan\delta = \frac{g'}{g}T_n = N\frac{fg'}{g}\left[1+\left(\frac{g'}{g}\right)^2\right]^{-1/2} \tag{31}$$

and

$$t_n = \frac{T_n}{N}, \quad t_t = \frac{T_t}{N}. \tag{32}$$

Here T_n could be identified from the measured rate of dissipation D specified by (30).

The general structure of constitutive equations presented in this section can now be used to formulate the friction and sliding rules for the various particular cases. We shall discuss these applications in Section 5.

4. MODELLING OF ANISOTROPIC WEAR

The specific wear rate is defined as the rate of material removal at the contact surface for a unit area. For an anisotropic friction condition this rate will vary with the orientation of the sliding velocity vector. A simple assumption can now be made, by postulating the wear rate to be function of dissipation rate along the sliding direction. In this way, the wear and friction characteristics are interrelated. Obviously, this assumption cannot be regarded as generally valid. For instance, the test results reported by Jacobs *et al.* (1990), or Miyoshi and Buckley (1982) indicate a close correlation between friction and wear properties. On the other hand, some of the test data of Sung and Suh (1979) concerned with the wear properties of fibre-reinforced composites do not exhibit this correlation. In fact, the wear rate can be greatly affected by damage evolution within the subsurface layer due to contact friction [see, for instance, Hornbogen (1986) and Berthier (1990) for a discussion of damage and wear modes]. In such cases, internal damage, contact wear and friction are interrelated in a more complex manner.

The specific wear rate is represented by the rate of evolution of contact surfaces along the normal direction. The simplest constitutive assumption can be made by requiring this rate to be proportional to the dissipation rate, thus

$$\dot{\varphi}_n = \dot{\boldsymbol{\varphi}}^+ \cdot \mathbf{n}^+ + \dot{\boldsymbol{\varphi}}^- \cdot \mathbf{n}^- = \dot{\varphi}_n^+ + \dot{\varphi}_n^- = (\gamma^+ + \gamma^-)D = \gamma v N \tilde{d}(\beta), \tag{33}$$

where $\dot{\boldsymbol{\varphi}}^+$, $\dot{\boldsymbol{\varphi}}^-$ are the rates of transformation vectors at the contact surfaces and $\dot{\varphi}_n^+$, $\dot{\varphi}_n^-$ are their normal components ($\mathbf{n}^+, \mathbf{n}^-$ being unit normals directed into the interior of contacting bodies). The respective wear parameters are γ^+ and γ^-, where $\gamma = \gamma^+ + \gamma^-$ represents the joint wear parameter. The wear function

$$j(\beta) = \frac{\dot{\varphi}_n(\beta)}{\gamma v N} = \tilde{d}(\beta) \tag{34}$$

represents the directional variation of wear rate on the sliding velocity orientation β.

The assumption (33) generalizes previous models by Archard (1953) or Zmitrowicz (1987) who did not relate explicitly wear and friction properties.

Relation (33) follows from the assumption on proportional dependence of the wear rate on the dissipation rate. A more general relation is obtained by postulating the wear function $j(\beta)$ to depend non-linearly on $\tilde{d}(\beta)$, thus

$$j(\beta) = [\tilde{d}(\beta)]^q, \tag{35}$$

where $q > 0$ is a wear exponent. The wear rate now is

$$\dot{\varphi}_n(\beta) = \gamma N v j(\beta) = \gamma N v [\tilde{d}(\beta)]^q. \tag{36}$$

An example of an application of this wear rule is presented in Fig. 6, where the

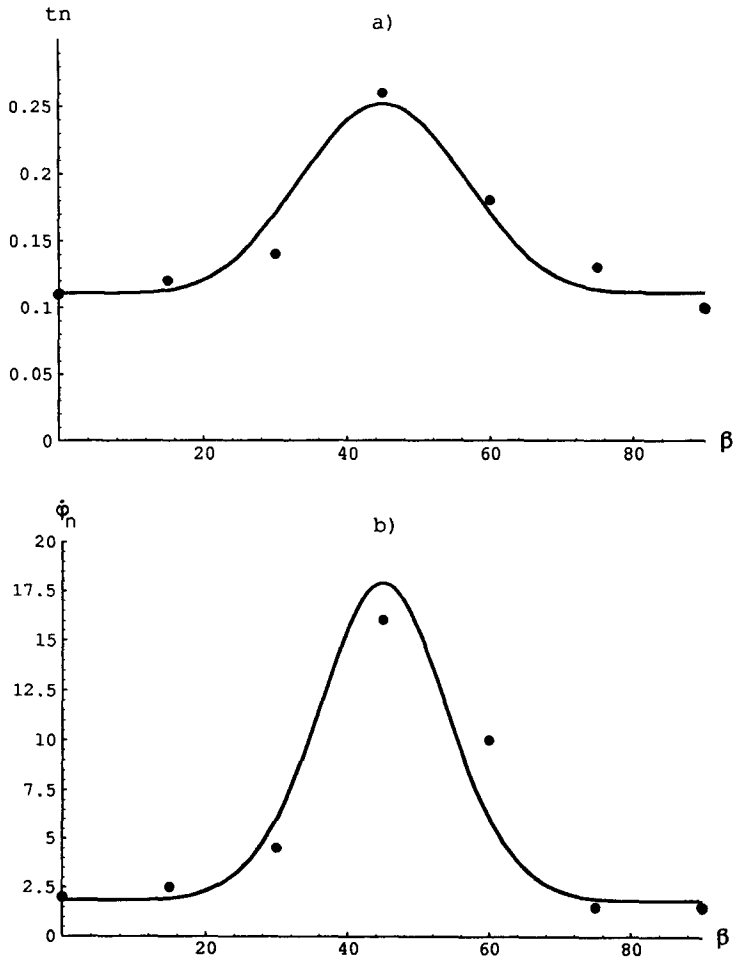

Fig. 6. Experimental data of Jacobs *et al.* (1990) fitted by functions (37): (a) friction coefficient $t_n(\beta)$ along the sliding velocity; (b) wear rate $\dot{\varphi}_n(\beta)$.

experimental data of Jacobs *et al.* (1990) concerned with friction and wear of fibre-reinforced composites are used. Figure 6(a) presents the variation of the friction coefficient $\mu_n = t_n = T_n/N$ specified by the force component T_n along the sliding velocity. The friction coefficient was averaged from peak to peak in oscillatory tests of an aluminium alloy pin sliding on a carbon-fibre/epoxy-resin laminate. The force was measured by inserting a quartz element along the sliding direction. It seems that the lateral force component was not determined. Note that variation of $t_n(\beta) = \tilde{d}(\beta)$ and the wear rate can be described by the relation

$$t_n(\beta) = a_1 + a_2(1-\cos\beta)^3$$
$$\dot{\varphi}_n(\beta) = a_3[t_n(\beta)]^q, \tag{37}$$

where $a_1 = 0.111$, $a_2 = 0.018$, $a_3 = 6.72$ and $q = 2.78$.

The presented wear model provides a very simple description, neglecting the evolution of friction anisotropy parameters due to wear and damage evolution within the contact layers.

In order to synthesize the description presented in this paper, let us introduce five fundamental diagrams specifying friction, dissipation and wear characteristics of contact surfaces.

(i) Limit friction curve, eqn (24)

$$t(\alpha) = \frac{T}{N} = f(\alpha). \tag{38}$$

(ii) Slip potential curve, eqn (26)

$$g = g(\alpha). \tag{39}$$

(iii) Non-dimensional dissipation function

$$\tilde{d}(\beta) = \frac{D}{Nv} = t_n(\beta) = \frac{T_n}{N} = f\left[1+\left(\frac{g'}{g}\right)^2\right]^{-1/2}. \tag{40}$$

(iv) Constant dissipation rate curve

$$\bar{v}(\beta) = \frac{v}{(D/N)} = \frac{1}{\tilde{d}(\beta)}. \tag{41}$$

(v) Wear function $j(\beta)$, eqn (35).

These fundamental diagrams are discussed for specific models considered in the next section.

5. SOME SPECIFIC FRICTION MODELS

5.1. *Orthotropic limit friction condition represented by an ellipse*

An elliptical friction condition was used by Ziemba (1952), Michałowski and Mróz (1978), Curnier (1984) and Zmitrowicz (1989). Following the main result of the model of asperity interaction discussed in Section 2, assume the limit friction condition and the sliding potential in the forms

$$F(T_x, T_y, N) = \left[\left(\frac{T_x}{c_1}\right)^2 + \left(\frac{T_y}{c_2}\right)^2\right]^{1/2} - N = 0, \quad 0 < \frac{c_2}{c_1} = m < 1$$

$$G(T_x, T_y, N) = \left[\left(\frac{T_x}{d_1}\right)^2 + \left(\frac{T_y}{d_2}\right)^2\right]^{1/2} - N = 0, \quad \frac{d_2}{d_1} = m^p, \quad 0 \leqslant p \leqslant 1, \tag{42}$$

where x, y follow the orthogonal orthotropy axes. The sliding potential has a different axes ratio to that of the limit friction ellipse. For $p = 1$, we have the associated sliding rule, $F = G$ and for $p = 0$ the sliding potential is a circle, predicting the sliding velocity coaxial with the friction force ($\alpha = \beta$). We have

$$v_x = \lambda \frac{\partial G}{\partial T_x} = \lambda \frac{T_x}{d_1^2 N}, \quad v_y = \lambda \frac{\partial G}{\partial T_y} = \lambda \frac{T_y}{d_2^2 N}, \tag{43}$$

where

$$\lambda = \frac{d_1^2}{c_1}[v_x^2 + (m^{2p-1} v_y)^2]^{1/2} = v \frac{d_1^2}{c_1}[\cos^2 \beta + (m^{2p-1} \sin \beta)^2]^{1/2}. \tag{44}$$

The friction force components are expressed as follows:

$$T_x = \frac{N c_1 \cos \beta}{[\cos^2 \beta + (m^{2p-1} \sin \beta)^2]^{1/2}}, \quad T_y = \frac{N c_1 m^{2p} \sin \beta}{[\cos^2 \beta + (m^{2p-1} \sin \beta)^2]^{1/2}} \tag{45}$$

or alternatively, the force components T_n along the sliding velocity and T_t normal to the velocity vector can be obtained from (45), namely

$$T_n = \frac{N c_1 (\cos^2 \beta + m^{2p} \sin^2 \beta)}{[\cos^2 \beta + (m^{2p-1} \sin \beta)^2]^{1/2}}, \quad T_t = \frac{N c_1 (1 - m^{2p}) \sin \beta \cos \beta}{[\cos^2 \beta + (m^{2p-1} \sin \beta)^2]^{1/2}}. \tag{46}$$

The relation between α and β takes now the form

$$\tan \beta = m^{-2p} \tan \alpha. \tag{47}$$

The representation (45) could be generalized to any orthogonal system x', y', not necessarily coinciding with the orthotropy axes x, y. Let us introduce two matrices C_{ij} and M_{ij} which in the orthotropy reference system x, y, have the diagonal forms

$$C_{ij}^0 = \begin{bmatrix} c_1 & 0 \\ 0 & c_2 \end{bmatrix}, \quad M_{ij}^0 = \begin{bmatrix} 1 & 0 \\ 0 & m^{2p-1} \end{bmatrix} \tag{48}$$

and in any rotated orthogonal system x', y', these matrices are

$$\mathbf{C} = \mathbf{Q}\mathbf{C}^0\mathbf{Q}^T, \quad \mathbf{M} = \mathbf{Q}\mathbf{M}^0\mathbf{Q}^T, \tag{49}$$

where $\mathbf{Q}$ is the plane orthogonal rotation matrix, $\mathbf{Q}^{-1} = \mathbf{Q}^T$, $\det \mathbf{Q} = 1$, thus

$$Q_{ij} = \begin{bmatrix} \cos \varphi & -\sin \varphi \\ \sin \varphi & \cos \varphi \end{bmatrix}, \tag{50}$$

where φ denotes the angle of rotation with respect to orthotropy axes. We shall call $\mathbf{C}$ the *orthotropy matrix* and $\mathbf{M}$ the *non-associativity matrix*. Introducing the matrix $(\mathbf{M}^2)_{ij} = M_{ik} M_{kj}$, the constitutive relations (45) can be expressed in any orthogonal system x', y' in the form

$$T_i = NC_{ij}M_{jk}\frac{v_k}{[v_l(\mathbf{M}^2)_{lm}v_m]^{1/2}}, \quad i,\ldots,m = 1, 2. \tag{51}$$

In particular, when $p = 1/2$, then $\mathbf{M} = \mathbf{M}^0 = \mathbf{1}$, and the relations (51) become

$$T_i = NC_{ij}\frac{v_j}{v}, \quad i, j = 1, 2 \tag{52}$$

and are equivalent to the form discussed extensively by Zmitrowicz (1989). It is seen that (52) constitutes only the particular case of a more general class of constitutive relations (51) for the orthotropic friction. The objectivity of (51) with respect to rotation of the reference system occurs. In fact for any rotation matrix $\mathbf{Q}$, the following transformation rules apply

$$\mathbf{T}^+ = \mathbf{QT}, \quad \mathbf{C}^+ = \mathbf{QCQ}^T, \quad \mathbf{M}^+ = \mathbf{QMQ}^T, \quad \boldsymbol{v}^+ = \mathbf{Q}\boldsymbol{v} \tag{53}$$

and the relation (51) is

$$\mathbf{T}^+ = \mathbf{QT} = N\frac{\mathbf{C}^+\mathbf{M}^+\boldsymbol{v}^+}{[\boldsymbol{v}^{+T}(\mathbf{M}^+)^2\boldsymbol{v}^+]^{1/2}} = N\frac{\mathbf{QCM}\boldsymbol{v}}{[\boldsymbol{v}^T\mathbf{M}^2\boldsymbol{v}]^{1/2}}. \tag{54}$$

The dissipation function is expressed as follows:

$$D = Nvc_1\frac{\cos^2\beta + m^{2p}\sin^2\beta}{[\cos^2\beta + (m^{2p-1}\sin\beta)^2]^{1/2}} = Nv\tilde{d}(\beta) \tag{55}$$

or using the general representation (51) in an arbitrary reference frame, we have

$$D = N\frac{\boldsymbol{v}^T(\mathbf{CM})\boldsymbol{v}}{[\boldsymbol{v}^T\mathbf{M}^2\boldsymbol{v}]^{1/2}} = Nv\frac{\boldsymbol{\rho}^T(\mathbf{CM})\boldsymbol{\rho}}{[\boldsymbol{\rho}^T\mathbf{M}^2\boldsymbol{\rho}]^{1/2}}, \tag{56}$$

where $\boldsymbol{\rho}$ is a normalized velocity vector, $\rho_i = v_i/v$.

The model presented involves three parameters describing both the limit friction and the sliding rule. In fact c_1 and c_2 are the principal friction coefficients along the orthotropy axes and p specifies the shape of sliding potential. In particular, when $p = 1$, the associated sliding rule results and $F = G$. This case was already discussed by Michałowski and Mróz (1978) and Curnier (1984). For $p = 1$, we have

$$\mathbf{C} = c_1\mathbf{M}, \quad \mathbf{CM} = c_1\mathbf{M}^2, \quad \mathbf{T} = Nc_1\frac{\mathbf{M}^2\boldsymbol{v}}{[\boldsymbol{v}^T\mathbf{M}^2\boldsymbol{v}]^{1/2}}. \tag{57}$$

These relations could easily be identified with those derived earlier in Michałowski and Mróz (1978) using orthotropy axes as the reference system.

Figure 7 shows the characteristic fundamental diagrams for the orthotropic friction model corresponding to different values of p.

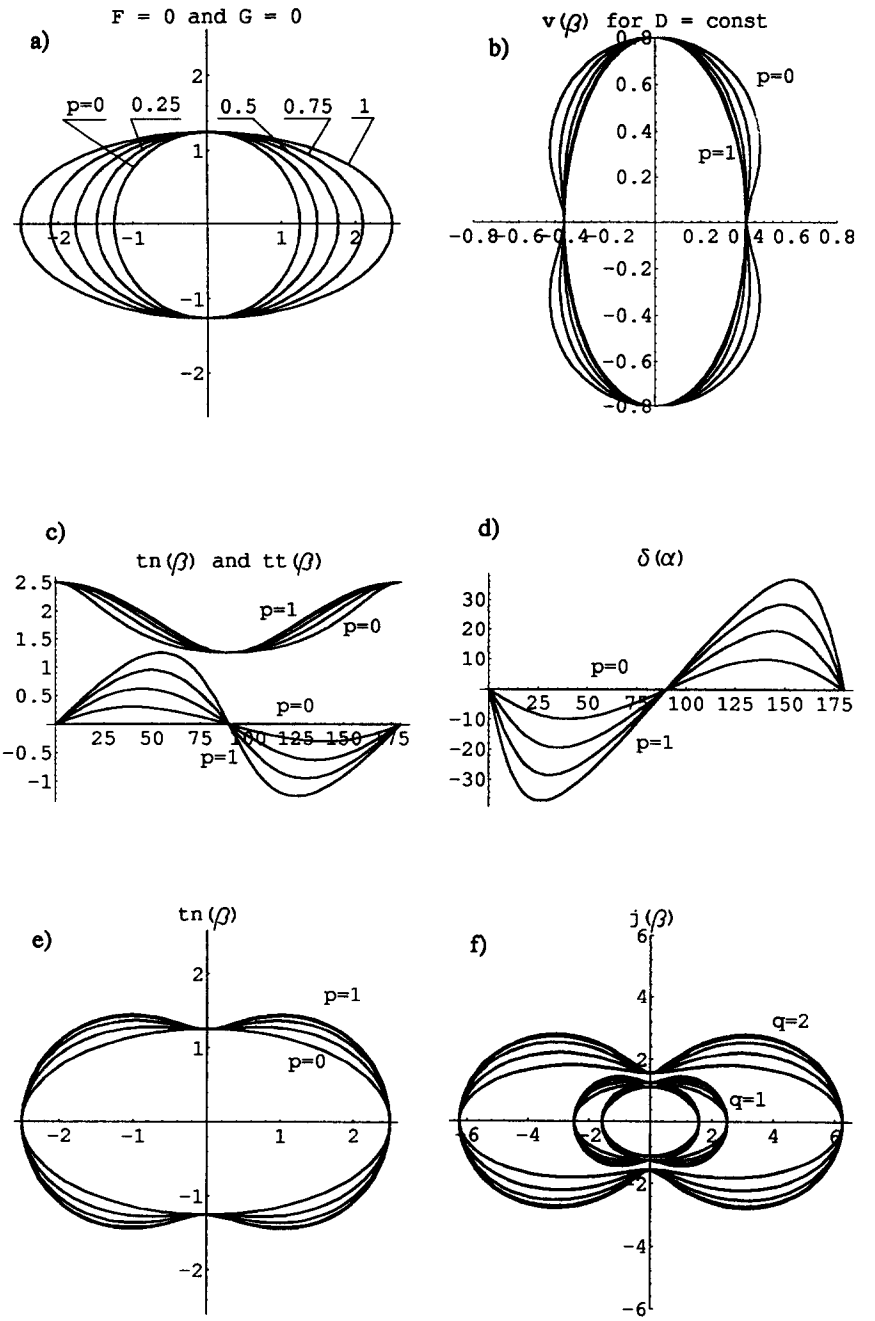

Fig. 7. Characteristic fundamental diagrams of the orthotropic friction model, eqn (42), for $m = c_2/c_1 = 1/2$ corresponding to different values of p: (a) limit friction curve $f(\alpha)$ and sliding potentials $g(\alpha)$, note, that for $p = 1$, $f(\alpha)$ and $g(\alpha)$ coincide; (b) constant dissipation rate curves $\bar{v}(\beta)$; (c) variation of t_n (upper diagrams) and t_t (lower diagrams) with direction β; (d) variation of inclination angle $\delta = \alpha - \beta$ with α; (e) non-dimensional dissipation function $\bar{d}(\beta) = t_n(\beta)$; (f) wear function $j(\beta) = [\bar{d}(\beta)]^q$ for $q = 0.5, 1, 2$.

5.2. *Superelliptic limit friction condition*

Consider the limit friction condition in the form

$$F(T_x, T_y, N) = \left[\left|\frac{T_x}{c_1}\right|^n + \left|\frac{T_y}{c_2}\right|^n\right]^{1/n} - N = 0, \tag{58}$$

where $1 \leqslant n < \infty$. For varying n the shape of the limit curve evolves from the parallelogram

($n = 1$) to the rectangle ($n \to \infty$), and for $n = 2$ the elliptic condition $(42)_1$ is obtained. The normality assumption results in the sliding rule

$$v_x = \dot{\lambda}\frac{\partial F}{\partial T_x}, \quad v_y = \dot{\lambda}\frac{\partial F}{\partial T_y}, \tag{59}$$

where

$$\dot{\lambda} = [|c_1 v_x|^{n/(n-1)} + |c_2 v_y|^{n/(n-1)}]^{(n-1)/n}. \tag{60}$$

The dissipation function now is expressed as follows:

$$D = N\dot{\lambda} = N[|c_1 v_x|^{n/(n-1)} + |c_2 v_y|^{n/(n-1)}]^{(n-1)/n}. \tag{61}$$

The inverse relations to (59) are now

$$T_x = \frac{\partial D}{\partial v_x}, \quad T_y = \frac{\partial D}{\partial v_y} \tag{62}$$

or explicitly

$$|T_x| = \frac{Nc_1|c_1 v_x|^{1/(n-1)}}{[|c_1 v_x|^{n/(n-1)} + |c_2 v_y|^{n/(n-1)}]^{1/n}}, \quad |T_y| = \frac{Nc_2|c_2 v_y|^{1/(n-1)}}{[|c_1 v_x|^{n/(n-1)} + |c_2 v_y|^{n/(n-1)}]^{1/n}} \tag{63}$$

and the following relation between directions of friction force and velocity vectors results

$$|\tan\beta| = \left(\frac{c_1}{c_2}\right)^n |\tan\alpha|^{n-1}. \tag{64}$$

An alternative, non-associated sliding rule for superelliptic friction condition (58) can be obtained by using the slip potential in the form of the ellipse $(42)_2$. Now (47) holds, and we have

$$T_x = \frac{Nc_1 v_x}{[|v_x|^n + m^{(2p-1)n}|v_y|]^{1/n}}, \quad T_y = \frac{Nc_2 m^{2p} v_y}{[|v_x|^n + m^{(2p-1)n}|v_y|]^{1/n}}, \tag{65}$$

where parameters m and p are defined by (42). The dissipation function is now

$$D = Nc_1 \frac{v_x^2 + m^{2p} v_y^2}{[|v_x|^n + m^{(2p-1)n}|v_y|]^{1/n}}, \tag{66}$$

however, the dissipation function (66) is not a potential for the constitutive relations (65), so the relations (62) do not occur.

5.3. *Sliding potential for an arbitrary limit friction condition*

The concept of different scaling of semiaxes of the sliding potential with respect to the limit friction condition can now easily be extended to any limit condition (24), namely

$$G(T_x, T_y, N) = T - N[f(\alpha)]^p = 0, \tag{67}$$

where $0 \leqslant p \leqslant 1$ for a convex limit friction condition $F = 0$ and $0 \leqslant p \leqslant p_{\max} < 1$ for a non-convex condition. In the latter case $p_{\max}$ is the largest value of p for which the sliding potential is convex.

In particular, when (67) is associated with the elliptical limit condition $(42)_1$, the resulting sliding potential does not exactly coincide with the potential $(42)_2$ but is very close to the scaled ellipse (Fig. 8).

Note that the form (67) of sliding potential preserves all symmetries of the limit friction condition. Our general expressions (24)–(31) can now easily be particularized by setting

$$g(\alpha) = [f(\alpha)]^p, \quad g'(\alpha) = p[f(\alpha)]^{p-1} f'(\alpha). \tag{68}$$

To illustrate the application of (67) and (68), consider the orthotropic limit friction condition represented by a superellipse, eqn (58), or in polar coordinates

$$F(T_x, T_y, N) = T - Nf(\alpha) = T - N\left[\left|\frac{\cos\alpha}{c_1}\right|^n + \left|\frac{\sin\alpha}{c_2}\right|^n\right]^{-1/n} = 0. \tag{69}$$

Figure 9 presents the characteristic diagrams (38)–(41), (35), and values of components T_n and T_t of the limit friction force T, cf. eqns (31), and the values of the angle δ, eqn (29). The above diagrams are shown for different values of model parameters p and q, describing the slip potential $g(\alpha)$ and the wear function $j(\beta)$, respectively.

In Fig. 10 some illustrative examples of characteristic diagrams are presented for the orthotropic friction condition in a form

$$f(\alpha) = \sum_{k=0}^{m} a_k \cos(2k\alpha). \tag{70}$$

To illustrate the application of (70), consider the experimental data of Casey and Wilks (1973) who studied the friction coefficient of a diamond crystal sliding on the (100) plane of the other diamond. The force component T_n was determined along the sliding velocity inclined at the angle β with respect to a selected reference orientation, while the lateral force component T_t was not specified. The cantilever beam system was used to measure the

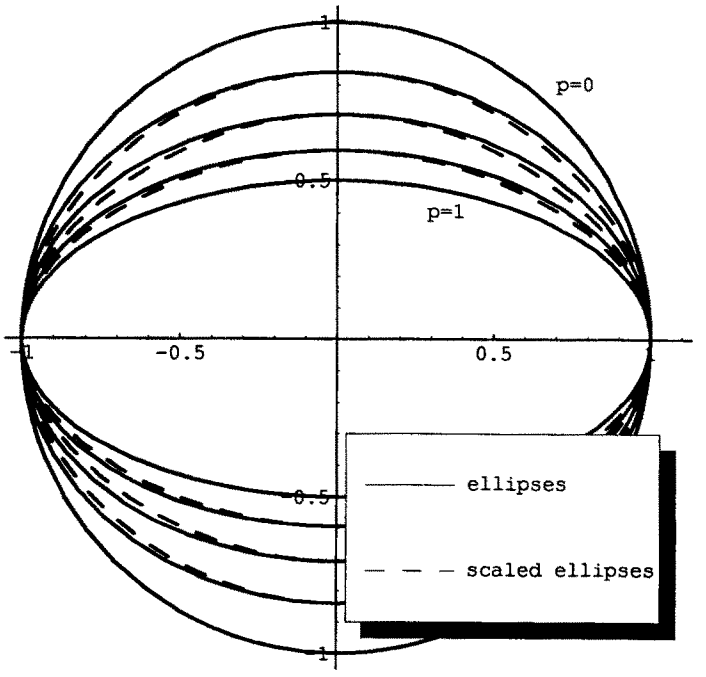

Fig. 8. Sliding potentials for different values of p resulting from (42) (ellipses) and from (67) (scaled ellipses).

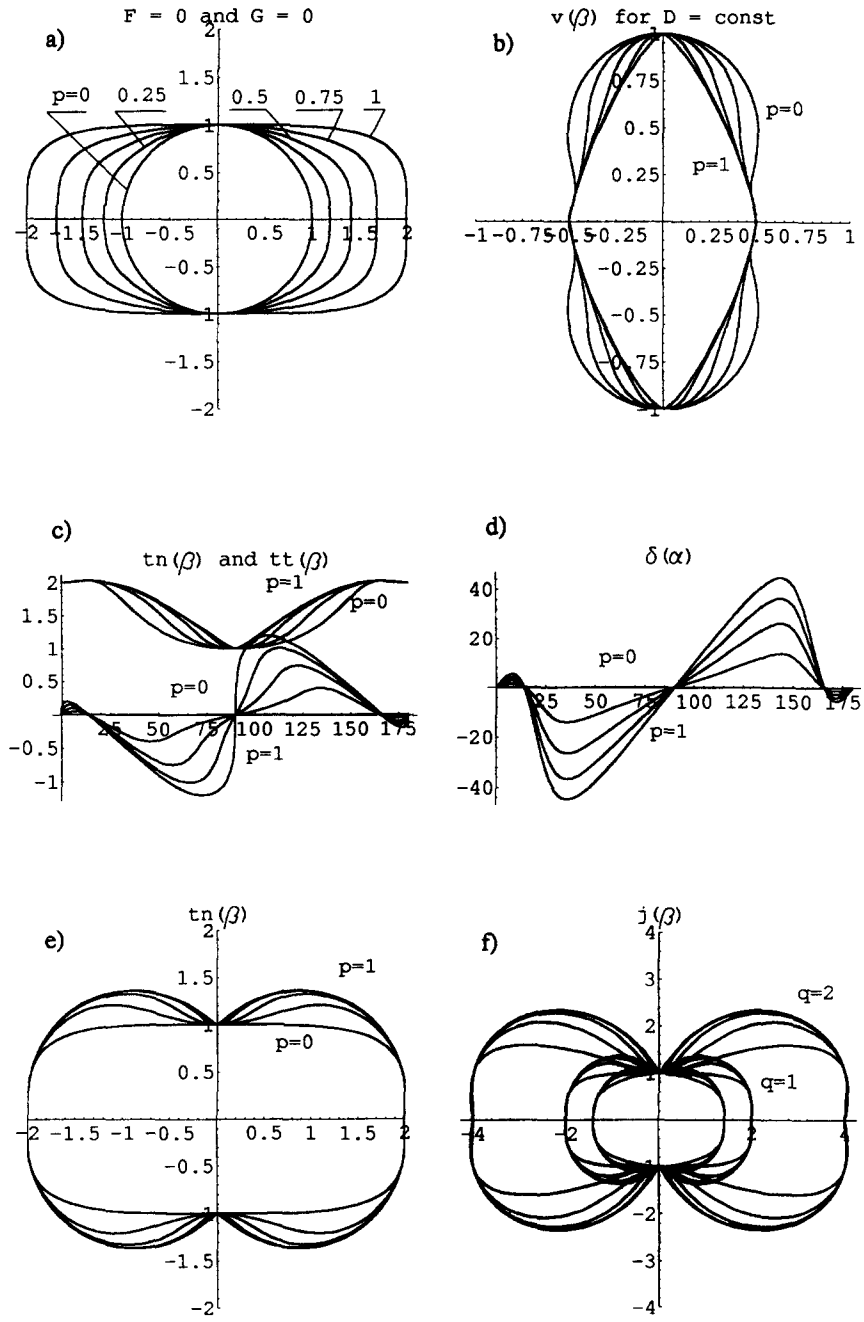

Fig. 9. Characteristic fundamental diagrams for the superelliptic friction condition, eqn (58), for $m = c_2/c_1 = 1/2$ and $n = 4$ corresponding to different values of p: (a) limit friction curve $f(\alpha)$ and sliding potentials $g(\alpha)$, note, that for $p = 1$, $f(\alpha)$ and $g(\alpha)$ coincide; (b) constant dissipation rate curves $\bar{v}(\beta)$; (c) variation of t_n (upper diagrams) and t_t (lower diagrams) with direction β; (d) variation of inclination angle $\delta = \alpha - \beta$ with α; (e) non-dimensional dissipation function $\bar{d}(\beta) = t_n(\beta)$; (f) wear function $j(\beta) = [\bar{d}(\beta)]^q$ for $q = 0.5, 1, 2$.

friction force. However, the beam deflection under this force provided only information on the force component normal to the beam (T_n). In order to simulate the data, the following form of $f(\alpha)$ was assumed

$$f(\alpha) = a_1 + a_2 \cos 4\alpha. \tag{71}$$

Next, for different values of the parameter p, the coefficients a_1 and a_2 were identified

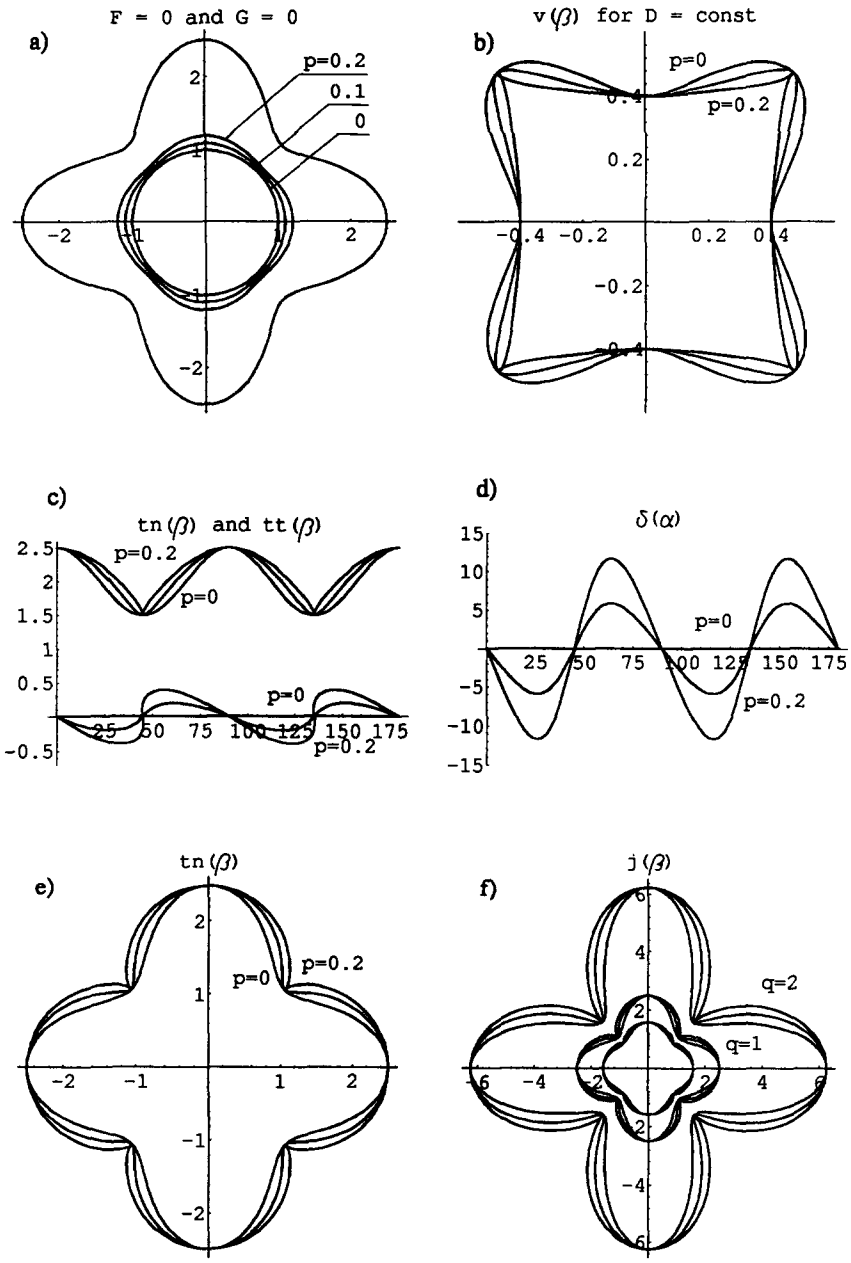

Fig. 10. Characteristic fundamental diagrams for the friction condition in the form $f(\alpha) = c_1 + c_2 \cos 2\alpha + c_3 \cos 4\alpha$, with $c_1 = 2$, $c_2 = 0$, and $c_3 = 0.5$ corresponding to different values of p: (a) limit friction curve $f(\alpha)$ and sliding potentials $g(\alpha)$; (b) constant dissipation rate curves $\bar{v}(\beta)$; (c) variation of t_n (upper diagrams) and t_t (lower diagrams) with direction β; (d) variation of inclination angle $\delta = \alpha - \beta$ with α; (e) non-dimensional dissipation function $\bar{d}(\beta) = t_n(\beta)$; (f) wear function $j(\beta) = [\bar{d}(\beta)]^q$ for $q = 0.5, 1, 2$.

in order to simulate $T_n(\beta)$ variation. Figures 11(a) and 11(b) present curves $T_n = T_n(\beta)$ and $f = f(\alpha)$ for the three values of p with optimal values of a_1 and a_2. It is seen that the response is not much sensitive to p and the set of parameters given in Table 1 provides fair description of the curve $T_n = T_n(\beta)$. The identification was only possible for $p < 0.1$ because of the requirement of convexity of the sliding potential $g(\alpha) = [f(\alpha)]^p$.

6. CONCLUDING REMARKS

A model of anisotropic friction was generated by considering a simple interaction of isotropic and orthotropic asperity systems. The general structure of constitutive relations

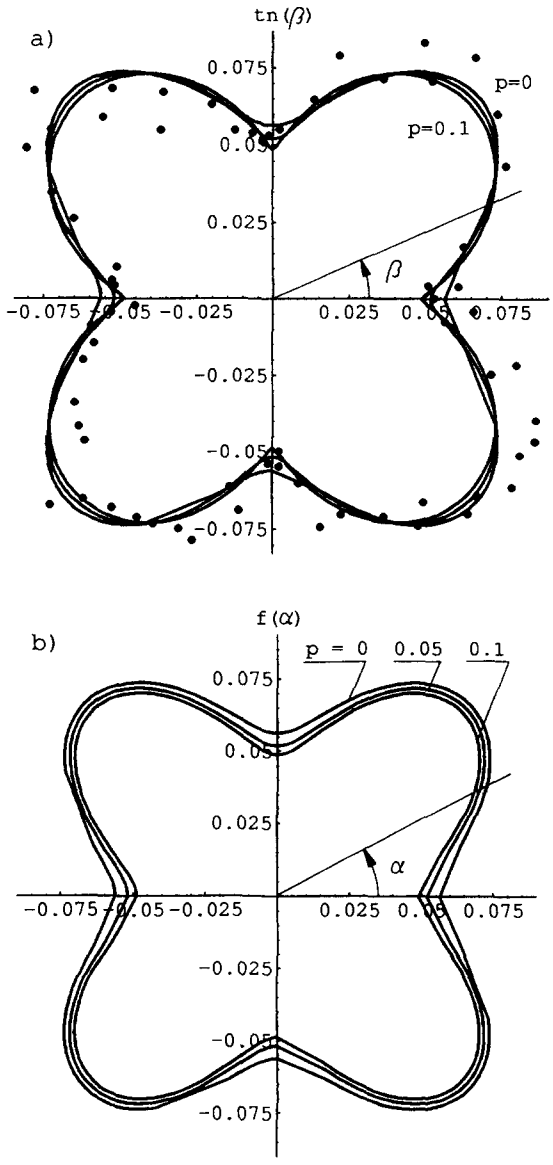

Fig. 11. Identification of the limit friction condition using experimental values of $t_n = t_n(\beta)$ (Casey and Wilks, 1973): (a) diagrams $t_n = t_n(\beta)$; (b) limit friction curves $t = f(\alpha)$.

provides a uniform framework in generating sliding rules, dissipation and wear characteristics starting from the limit friction condition. Several fundamental diagrams can be generated by following these constitutive rules. However, a more complete set of experimental data are required in order to verify the constitutive assumptions and to identify the material parameters specifying friction, sliding and wear effects. The extension to more general rules, accounting for normal compliance and plastic effects, could be provided within the proposed formulation, which constitutes a generalization of previous results presented in Curnier (1984), Michałowski and Mróz (1978) and Zmitrowicz (1989).

Table 1

p	a_1	a_2
0.00	0.07521	−0.01896
0.05	0.07207	−0.02023
0.10	0.06963	−0.02080

REFERENCES

Archard, J. F. (1953). Contact and rubbing of flat surfaces. *J. appl. Phys.* **24,** 981–988.
Berthier, Y. (1990). Experimental evidence for friction and wear modelling. *Wear* **139,** 77–92.
Casey, M. and Wilks, J. (1973). The friction of diamond sliding on polished cube faces of diamond. *J. Phys. D: Appl. Phys.* **6,** 1772–1781.
Curnier, A. (1984). A theory of friction. *Int. J. Solids Structures* **20,** 637–647.
Haessig Jr, D. A. and Friedland, B. (1991). On the modelling and simulation of friction. *J. Dynamic Systems, Measurement Control, ASME* **113,** 354–362.
Halaunbrenner, M. (1960). Directional effects in friction. *Wear* **3,** 421–425.
Hornbogen, E. (1986). Description and wear of materials with heterogeneous and anisotropic microstructures. *Wear* **111,** 391–402.
Jacobs, O., Friedrich, K., Marom, G., Schulte, K. and Wagner, H. D. (1990). Fretting wear performance of glass-, carbon-, and aramid–fibre/epoxy and PEEK composites. *Wear* **135,** 207–216.
Jarzębowski, A. and Mróz, Z. (1994). On slip and memory rules in elastic, friction contact problems. *Acta Mechanica* **102,** 199–216.
Michałowski, R. and Mróz, Z. (1978). Associated and non-associated sliding rules in contact friction problems. *Arch. Mech.* **30,** 259–276.
Miyoshi, K. and Buckley, D. H. (1982). Anisotropic tribological properties of SiC. *Wear* **75,** 253–268.
Mróz, Z. and Jarzębowski, A. (1994). Phenomenological model of contact slip. *Acta Mechanica* **102,** 59–72.
Oden, J. T. and Martins, J. A. C. (1985). Models and computational methods for dynamic friction phenomena. *Comp. Meth. Appl. Mech. Engng* **52,** 527–634.
Rabinowicz, E. (1957). Direction of the friction forces. *Nature* **179,** 1703.
Sung, N. and Suh, N. (1979). Effect of fiber orientation on friction and wear of fiber reinforced polymeric composites. *Wear* **53,** 129–141.
Ziemba, S. (1952). On certain cases of anisotropic friction. *Arch. Mech.* **4,** 105–121 (in Polish).
Zmitrowicz, A. (1987). A thermodynamical model of contact, friction and wear: I governing equations, II constitutive equations for materials and linearized theories, III constitutive equations for friction, wear and frictional heat. *Wear* **114,** 135–168, 169–197, 199–221.
Zmitrowicz, A. (1989). Mathematical descriptions of anisotropic friction. *Int. J. Solids Structures* **25,** 837–862.